Retrieval of the ground dielectric permittivity by planetary GPR accommodated on a rover: Application to the estimation of the reflectors' depth by the WISDOM/ExoMars radar

Nicolas Oudart, Valérie Ciarletti, Alice Le Gall, Yann Herve, Emile Brighi

Planetary and Space Science 224 (2022) 105606

Contents lists available at ScienceDirect

Planetary and Space Science

journal homepage: www.elsevier.com/locate/pss

Retrieval of the ground dielectric permittivity by planetary GPR accommodated on a rover: Application to the estimation of the reflectors' depth by the WISDOM/ExoMars radar

Nicolas Oudart [a,*], Valérie Ciarletti [a], Alice Le Gall [a,b], Yann Hervé [a], Emile Brighi [a]

[a] LATMOS/IPSL, UVSQ Université Paris-Saclay, Sorbonne Université, CNRS, France
[b] Institut Universitaire de France (IUF), Paris, France

A B S T R A C T

Sounding radars, also called Ground Penetrating Radars (GPR), have unlocked a third dimension in planetary exploration, offering the possibility to remotely investigate the subsurface of a planetary object. In the last decade, the increasing developments in the robotic exploration of the Moon and Mars have allowed the accommodation of GPR on rovers. As such, they can perform soundings at the local scale, directly from the surface. This led to the selection of two Lunar and three Martian GPR instruments on board 5 different rovers. The interpretation of GPR soundings in terms of distances between buried interfaces/structures, and the nature of subsurface materials requires the knowledge of the velocity of the electromagnetic wave in the subsurface. This latter depends on the ground dielectric permittivity with is commonly derived from the shape of diffraction curves, if any, in the acquired radargrams. In this work we propose an automatized technique based on the Hough transform designed to detect and characterize diffraction curves. All planetary GPR to this day being "air-coupled" (with antennas a few decimeters above the surface for safety and mobility reasons), the proposed technique accounts for refraction at the surface. It is now included in the data processing and interpretation chain of WISDOM, the GPR of the Rosalind Franklin ExoMars rover. The technique was validated on both synthetic and experimental WISDOM radargrams.

1. Introduction

The robotic exploration of the Moon and Mars allows the study of geological sites at the local scale, with instrumented robotic vehicles named « robotic rovers ». If originally Lunar and Martian robotic rovers could only explore the surface or at best the very first top centimeters, the subsurface is now their new target of interest. Indeed, the subsurface holds essential information to better understand the geological history of the investigated site and nearly all robotic rovers now carry a Ground Penetrating Radar (GPR) to explore it. In particular, a GPR is on board all Lunar and Martian rover missions of the last decade: the LPR instruments of the Yutu (Fang et al., 2014) and Yutu 2 (Jia et al., 2018) rovers (Chang'E 3 and Chang'E 4 lunar missions, China National Space Administration), the RIMFAX instrument (Hamran et al., 2020) of the Perseverance rover (Mars 2020 mission, National Aeronautics and Space Administration), the RoSPR (later named RoPeR) instrument (Zhou et al., 2020) of the Zhurong rover (Tianwen-1 mission, CNSA), and the WISDOM instrument (Ciarletti et al., 2017) of the Rosalind Franklin rover (ExoMars rover mission, European Space Agency). GPR have the ability to unveil the structure and average composition of the subsurface below the rover, by providing radar images named "radargrams", that are generated by a series of radar traces acquired along the rover path.

However, GPR radar traces are not self-consistent: as echoes from buried interfaces or scatterers are characterized by their time-delays, an additional information on the subsurface electrical properties (namely its dielectric permittivity or permittivity) is required to convert these propagation times into propagation distances travelled in the subsurface, and by extension into depths. Knowing the ground dielectric permittivity also provides insights into the subsurface composition and porosity. In the context of planetary GPR investigation, two main techniques are commonly used to estimate the subsurface dielectric permittivity: it can be estimated from the surface reflectivity (Ciarletti et al., 2017; Dorizon et al., 2016; Hervé et al., 2020) or from the shape of the diffraction curves (see definition below) present in radargrams. The former technique requires an accurate radiometric calibration of the instrument. It relies on measurements performed on targets of well-known reflectivity on Earth and also on a good knowledge of the instrument sensitivity to parameters such as temperature (in order to properly correct the data amplitude). In addition, this method is only applicable in the case of a smooth surface and provides a permittivity value that may be representative of only the upper shallow layer of the subsurface (a few centimeters in the case of WISDOM). These are the reasons why the characterization of diffraction curves is often favored (Ding et al., 2021; Lai et al., 2016, 2019).

A "diffraction curve" is the name given to the pattern formed by

* Corresponding author.
E-mail address: nicolas.oudart@latmos.ipsl.fr (N. Oudart).

https://doi.org/10.1016/j.pss.2022.105606
Received 20 May 2022; Received in revised form 1 October 2022; Accepted 14 November 2022
Available online 17 November 2022

echoes arising from a point-like reflector in a radargram. A reflector is considered "point-like" if its dimensions are small with respect to the GPR wavelengths in the subsurface. On Earth, where most GPR are operated with antennas in contact with the surface, a configuration named "ground-coupled", this pattern is a mathematic hyperbola, which shape depends on the velocity of the waves in the sounded medium. For a homogeneous and non-magnetic medium with low electrical losses, the waves' velocity is given by $c/\sqrt{\varepsilon}$ where c is the speed of light in vacuum and ε the real part of the relative dielectric permittivity of the material surrounding the reflector, relative to that of vacuum. If ε is in theory frequency-dependent, the effect of frequency is expected to be small over a GPR spectrum, and for simplicity this parameter is named "dielectric permittivity" in the following.

By detecting and fitting diffraction curves present in a radargram, the propagation speed of electromagnetic waves in the subsurface can be estimated and thus the permittivity value retrieved. However, for obvious safety and navigation reasons, all aforementioned planetary GPR have their antennas tens of centimeters above the surface, a configuration named "air-coupled", leading to diffraction curves that are not perfect hyperbolas due to wave refraction at the surface. Diffraction curves in the radargrams from the LPR instruments of the Yutu rovers were thus fitted manually (Lai et al., 2016) to infer an average dielectric permittivity (of a mixture of air and subsurface) then considered as a first approximation of the ground dielectric permittivity.

In this study, we propose a method to automatically detect and characterize diffraction curves in "air-coupled" planetary GPR radargrams, in order to estimate dielectric permittivity values of the subsurface.

The proposed technique is validated on data (either synthetic or experimental) corresponding to the WISDOM (Water Ice Subsurface Deposits Observation on Mars) GPR of the Rosalind Franklin rover, which is operating on a broad frequency bandwidth from 0.5 to 3 GHz (i.e. wavelength from 10 to 60 cm in vacuum). The Rosalind Franklin rover of the ExoMars mission has been designed to search for potential traces of life in the Martian shallow subsurface, an environment less hostile than the surface. WISDOM has been selected to sound the subsurface of the rover landing site, Oxia Planum (Vago et al., 2017). The characterization of diffraction curves in WISDOM radargrams will serve the mission objectives (Ciarletti et al., 2017) on three different aspects: (i) The ExoMars rover will collect samples down to 2 m in the Martian subsurface, where preserved biomarkers could potentially be present. WISDOM will guide the selection of a relevant underground target which requires an accurate estimation of distances in the subsurface, and thus an accurate estimation of the GPR signal propagation speed. (ii) The samples will be collected in the subsurface with a drill. To avoid any hazards which may damage the drill, detecting buried rocks is essential. Since the signature of these latter are diffraction curves, the automatic detection of diffraction curves on WISDOM radargrams will guarantee safe drilling operations. (iii) The dielectric permittivity of subsurface materials provides clues on their composition. One of the objectives of WISDOM being to unveil the geological history of its landing site, any information on the subsurface composition is of prime importance. However, the proposed method is applicable to any "air-coupled" GPR, operated on the Earth, Mars or on the Moon.

In the following, we first introduce the diffraction curve model (section II), as well as the technique (section III) we selected for the diffraction curve detector. This technique is based on the Hough transform, a shape detector widely-known in image processing. We then validate the technique on synthetic WISDOM radargrams (section IV), generated by a Finite Differences in Time-Domain (FDTD) numerical code, and apply it on experimental WISDOM radargrams (section V), acquired in an icy environment for which the electrical properties are well constrained. Section VI is dedicated to a discussion on the limitations and perspective of the proposed technique.

2. Diffraction curves models

In the present study we consider the following hypotheses to model diffraction curves: we consider a buried point-like reflector at a horizontal position X along the GPR traverse path, and a depth Z in a homogeneous subsurface layer (see Figs. 1 and 2). The subsurface is lossless, of dielectric permittivity ε. The GPR configuration is monostatic, with a single point of transmission/reception (Tx/Rx) for the signal. The point source is considered omnidirectional (no aperture of the antenna radiation pattern considered here).

Two different geometrical models for the time-delays of echoes from this buried reflector can then be drawn depending on the GPR antenna set-up: "ground-coupled" (antenna in contact with the ground) or "air-coupled" (antenna in the air, typically a few decimeters above the ground).

2.1. "Ground-coupled" GPR

In the case of antennas directly coupled to the surface (the usual case on Earth, shown in Fig. 1), the propagation time T back and forth between the antennas and the reflector can easily be determined for every horizontal position x of the antennas on the surface as

$$T(x) = \frac{2\sqrt{\varepsilon}}{c}\sqrt{(x-X)^2 + Z^2} \tag{1}$$

We can identify equation (1) as being the equation of a mathematic hyperbola, which can be re-written as follows:

$$T^2(x) = \alpha + \beta(x-\gamma)^2 \tag{2}$$

where

$$\begin{cases} \alpha = \left(\frac{2\sqrt{\varepsilon}}{c}Z\right)^2 = T^2(X) \\ \beta = \frac{4\,\varepsilon}{c^2} \\ \gamma = X \end{cases}$$

The position of the hyperbola's apex depends on α and γ, and the slope of the hyperbola for large values of $(x-X)$ depends on β. The dielectric permittivity ε of the subsurface and the position of the reflector in the subsurface (X, Z) can be readily retrieved by fitting equation (1) to the diffraction curve, as only one combination of the α, β and γ parameters values is possible for a given hyperbola.

A mathematic hyperbola is defined by three parameters. As a consequence, at least 3 points on a hyperbolic diffraction curve are in theory required to determine these parameter values. If we consider three distinct points L, M and N of coordinates (i_L, j_L), (i_M, j_M) and (i_N, j_N), the parameters α, β and γ of the unique hyperbola passing through these points can be expressed as follows:

$$\begin{cases} \gamma = \dfrac{(j_L{}^2 - j_M{}^2)i_N{}^2 - (j_L{}^2 - j_M{}^2)i_L{}^2 + (j_L{}^2 - j_N{}^2)i_L{}^2 - (j_L{}^2 - j_N{}^2)i_M{}^2}{2\left((j_L{}^2 - j_M{}^2)i_N - (j_L{}^2 - j_M{}^2)i_L + (j_L{}^2 - j_N{}^2)i_L - (j_L{}^2 - j_N{}^2)i_M\right)} \\ \beta = \dfrac{j_L{}^2 - j_M{}^2}{(i_L-\gamma)^2 - (i_M-\gamma)^2} \\ \alpha = j_L{}^2 - \beta(i_L-\gamma)^2 \end{cases} \tag{3}$$

With a « ground-coupled » GPR set-up, and in the retained hypotheses, we thus obtain a diffraction curve model which can in theory be easily inverted. Hence the intensive use of diffractions curves to estimate the dielectric permittivity of the subsurface on Earth. In practice, when manually fitting a hyperbolic diffraction curve, more than three points are usually considered because a measured diffraction curve is rarely an exact mathematical hyperbola.

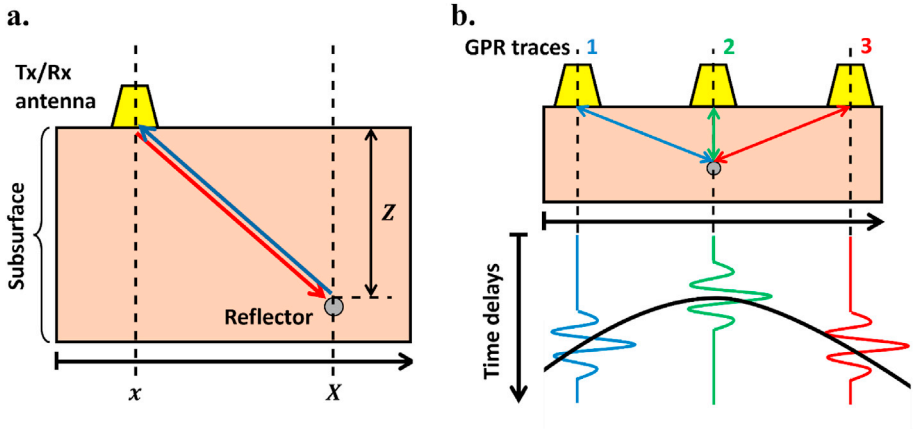

Fig. 1. (a) Geometrical propagation model used for GPR signals in the case of ground-coupled antennas, (b) Principle of a hyperbolic diffraction curve. The aperture of the antenna radiation pattern has been here exaggerated.

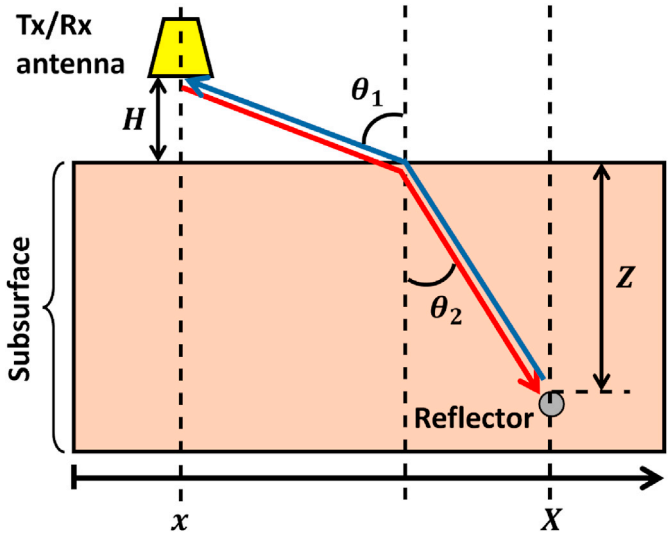

Fig. 2. Geometrical propagation model used for GPR signals in the case of air-coupled antennas. The aperture of the antenna radiation pattern has been here exaggerated.

2.2. "Air-coupled" GPR

In the case of antennas located at a given height H above the surface (as illustrated in Fig. 2, with $H = 38$ cm in the case of WISDOM), electromagnetic waves transmitted by the GPR are first refracted at the surface, at a position x_{ref} named "refraction point", before being transmitted to the subsurface. θ_1 and θ_2 correspond respectively to the incident and transmitted angles.

In this situation, the propagation time of electromagnetic waves T between the antennas and the reflector is determined for any horizontal position x of the antennas on the surface along the GPR transverse path as

$$T(x) = \frac{2}{c}\sqrt{(x_{ref} - x)^2 + H^2} + \frac{2\sqrt{\varepsilon}}{c}\sqrt{(X - x_{ref})^2 + Z^2} \quad (4)$$

This is no longer the equation of a mathematic hyperbola, and equation (4) cannot be easily inverted as x_{ref} is a function of x.

x_{ref}, the refraction point for a horizontal position x of the GPR antennas, is related to x and to the location of the reflector (X, Z) in the subsurface through the Snell-Descartes law:

$$\sin(\theta_1) = \sqrt{\varepsilon}\,\sin(\theta_2) \quad (5)$$

which can also be written:

$$\frac{|x - x_{ref}|}{\sqrt{(x - x_{ref})^2 + H^2}} = \frac{\sqrt{\varepsilon}\,|x_{ref} - X|}{\sqrt{(x_{ref} - X)^2 + Z^2}} \quad (6)$$

In a theoretical study on air-coupled GPR, Persico et al. (2015) further show that equation *(6)* is equivalent to a 4th degree equation, namely:

$$\begin{aligned} &x_{ref}^4 - 2(x+X)x_{ref}^3 + \left(x^2 + X^2 + 4xX + \frac{c^2(t_2^2 - \varepsilon^2 t_1^2)}{4(1-\varepsilon)\varepsilon}\right)x_{ref}^2 \\ &- \left(2x^2X + 2xX^2 + \frac{c^2 t_2^2}{2\varepsilon(1-\varepsilon)}x - \frac{c^2\varepsilon\, t_1^2}{2(1-\varepsilon)}X\right)x_{ref} + x^2x_0^2 \\ &+ \frac{c_0^2 t_2^2 x^2}{4\varepsilon(1-\varepsilon)} - \frac{c^2\varepsilon\, t_1^2 X^2}{4(1-\varepsilon)} = 0 \end{aligned} \quad (7)$$

where $t_1 = \frac{2H}{c}$ and $t_2 = \frac{2\sqrt{\varepsilon}Z}{c}$ are the time delays corresponding to a distance H travelled in the air and a distance Z travelled in the medium of dielectric permittivity ε, respectively. The analytical solutions of this equation are determined in the same study where it is demonstrated that only one solution is physically possible.

It is therefore theoretically possible in an "air-coupled" set-up to determine the dielectric permittivity ε of the subsurface, as well as the position (X, Z) of the reflector in the subsurface by fitting the corresponding diffraction curve. However, the inversion of the resulting model is not straightforward. We use a Nelder-Mead optimization algorithm (Nelder and Mead, 1965) to fit a diffraction curve in an "air-coupled" GPR set-up such as WISDOM's as described in section III.

Prior to that we use an automated diffraction curve detector based on the Hough transform (Hough, 1964) to detect diffraction curves in WISDOM radargrams. Indeed, manually fitting diffraction curves and inverting the corresponding (X, ε, Z) can be a long and repetitive process, with many sources of errors. In the frame of the ExoMars rover operations (and other planetary rover operations), decisions must be taken in a limited amount of time, and confidently. Automated diffraction curve detectors allow to objectively and rapidly detect and characterize these patterns in radargrams. Further, the Hough transform is a proven method, easily adaptable to any GPR diffraction curves, and not requiring any training dataset.

3. A hough transform approach

The Hough transform is a shape detector invented by Paul Hough in 1959 (US patent 3069654) and widely used in image processing. While the original Hough transform only allowed the detection of lines in an image, the technique was generalized by Duda and Hart (1972) to any shape that can be analytically defined. In particular, the Hough transform

has been successfully adapted for the detection of hyperbolic diffraction curves in ground-coupled GPR radargrams by Capineri et al. (1998) and, indeed, it has facilitated the interpretation of radargrams for many GPR applications on Earth, such as land mines detection (Carlotto, 2002), buried pipes diameter estimation (Windsor et al., 2005), or tree-roots observations (Li et al., 2016). To our knowledge, the present work proposes the first application of the Hough transform to the detection of diffraction curves in planetary air-coupled GPR radargrams.

In its adaptation to detect hyperbolas in images, the Hough transform follows this process:

- The surface echo, antenna coupling and any clutter constant over the radargram's horizontal axis is filtered by the subtraction of a free-space measurement and/or the mean value computed on the set of measurements (for more details see Hervé et al., 2020).
- An edge detection algorithm is applied to the image. In the case of radargrams, it allows the automatic detection of significant echoes. All the points in the radargram belonging to these detected edges are selected for the following steps. The edge detection technique we implemented is a simple peak detection applied to each radar trace, with a minimum time delay of 0.5 ns between two peaks, and threshold on the peaks' intensity. This threshold is selected depending on the level of noise expected in the radargram, and the maximum number of points allowed by the user for the Hough transform process (computation time increases exponentially with the number of points). For this study, a value of 20 dB below the maximum amplitude in the radargram was set as the threshold.
- Each possible triplet of points, chosen among the set of points identified in the previous step, defines an hyperbola. A 3D accumulator is incremented by one at the position corresponding to the values of the parameters (α,β,γ) of this hyperbola.
- Finally, local maxima within a 3D Moore neighborhood in the accumulator are identified. They correspond to hyperbolas actually present in the radargram. A threshold is applied to avoid false positives. In the theoretical case of a homogeneous loss-less subsurface, the precision on the estimated parameters of each detected diffraction curve is driven by the discretization steps $d\alpha$, $d\beta$ *and* $d\gamma$ in the 3D accumulator. In the experimental case, these steps must be chosen as a compromise between the desired precision on X, Z and ε and the need to have clear local maxima. Contributions from a same diffraction curve could indeed be divided into different (α,β,γ) values around the true parameters due to estimation errors if the accumulator steps are too small.

The main advantage of the Hough transform over machine learning techniques is that no training with a relevant dataset of diffraction curves is required (Hervé, 2018). Such a dataset is indeed difficult to obtain, as the waveform of echoes constituting a diffraction curve is variable depending on the sounded subsurface.

The main drawback of the technique is its execution time, which increases rapidly when testing all possible triplets of points in the detected contours of the radargram. For this reason, it is common with the Hough transform not to consider all possible triplets of points, but instead to use a statistically representative number of randomly selected triplets. To determine this number K, we use the criterion proposed by Xu and Oja (1993):

$$K = p\,\frac{N^3}{27} \tag{8}$$

where N is the total number of points, and p is a coefficient between 10 and 100.

Lastly, to adapt the Hough transform to diffraction curves obtained in an air-coupled GPR set-up, for each considered triplet of points the curve passing through is determined with the model presented in equation (4), and the Nelder-Mead optimization algorithm. To avoid solutions not physically possible, the optimization algorithm is initialized by the values of (α,β,γ) obtained with equation (3), and the plausibility of the solution found by the Nelder-Mead algorithm is checked before incrementing the 3D accumulator. The structure of the algorithm is detailed in Fig. 3.

Due to the accumulation process in the Hough transform, the uncertainties on the diffraction curves horizontal position, time delays and dielectric permittivity estimations presented in this work are only the uncertainties related to the precisions chosen for the Hough transform 3D accumulator (dt,dx,dε). For depth values, the uncertainty is derived from the dt and dε values and the formula $Z = \frac{2\sqrt{\varepsilon}}{c\,t}$. These are only partial uncertainties, as for each triplet of points fitted, all effects not accounted for in the diffraction curve model will lead to estimation errors.

4. Validation on synthetic WISDOM radargrams

In order to validate the Hough transform technique described in Section III, we generate synthetic WISDOM radargrams for a subsurface harboring multiple reflectors. The synthetic radargrams are generated using a Finite Differences in Time-Domain (FDTD) code named TEMSI-FD (Ciarletti et al., 2017) which includes a representative model of the WISDOM antennas and of the waveform of the transmitted signals. The waveform is a sine-Gaussian model of the WISDOM equivalent impulse in time-domain, experimentally determined on calibration target (the pulse-width is 0.3 ns and the central frequency of 1.75 GHz, Hervé et al., 2020; Hervé, 2018 for more details). TEMSI-FD was developed at XLIM, France; it includes absorbing boundary conditions with Perfectly Matched Layers that eliminate as much as possible the parasitic reflections occurring at the limit of the computational volume. It is also able to take into account non-homogeneous environments.

We consider one 4 m-long WISDOM traverse, with radar traces acquired every 10 cm (as planned once on Mars in the frame of the ExoMars mission), over a homogeneous subsurface of dielectric permittivity $\varepsilon = 4$ (a typical value for dry sandstones). Five spherical metallic reflectors are buried in the subsurface. Their diameter is 10 cm, a compromise between the maximum size at which a reflector can be considered as “point-like” for WISDOM (between 5 and 30 cm in a subsurface of $\varepsilon = 4$), and the size of cells in our subsurface model (with a typical numerical cell size of 5 mm, such spheres can be regarded as smooth). Furthermore, three of the metallic spheres are right below the antennas ground track (sphere number 1, 2 and 3), while the two others are off-track (sphere number 4 and 5).

It must be noted that metallic targets are obviously not representative of rocks expected in the Martian subsurface. Metallic targets are obviously more reflective than lithic ones, leading to echoes of higher amplitudes. However, the shape of the diffraction curves is unaffected by the reflector's composition, which is all that is required to test the Hough transform technique.

Table 1 summarizes the position of the different reflectors in the subsurface, namely their horizontal position X and “equivalent” depth Z in the material that is the shortest distance between the antenna and the reflector. For a reflector just below the GPR track, Z corresponds to the actual depth; which is not the case for an off-track reflector.

Fig. 5 displays the simulated radargram obtained by FDTD. The 5 diffraction curves corresponding to the five buried reflectors are clearly visible. The indicated time delay values are relative to the surface echo, which is the strongest signal visible at the top of the radargram. An edge detection algorithm is applied to the radargram (see Fig. 5, right). Points on the diffraction curves and their repetitions from multiple reflections are well detected. This set of points is used as the entry of the Hough transform.

Both the classic Hough transform for mathematic hyperbolas, and the Hough transform we adapted to account for refraction at the surface (hereafter referred to as the “corrected Hough transform”) is applied to the previously obtained set of points. The selected precision steps in the

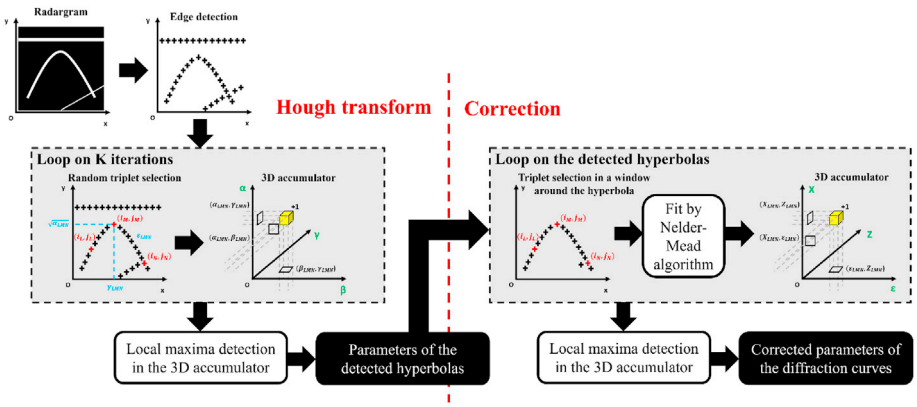

Fig. 3. Steps of the corrected Hough algorithm.

Table 1
Dielectric permittivity, horizontal positions and equivalent depths in the subsurface of the buried reflectors of the model, along with Hough transform estimations for the radargram shown in Fig. 6.

	True values			Classic Hough transform estimation			Corrected Hough transform estimation		
N°	X (m)	Z (m)	ε	X (m)	Z (m)	ε	X (m)	Z (m)	ε
1	1	1	4	0.95 ± 0.05	1.43 ± 0.05	2.0 ± 0.1	0.95 ± 0.05	0.99 ± 0.02	4.2 ± 0.1
2	2	1.5	4	1.95 ± 0.05	2.01 ± 0.06	2.3 ± 0.1	1.95 ± 0.05	1.56 ± 0.03	3.8 ± 0.1
3	3	0.5	4	2.95 ± 0.05	0.85 ± 0.05	1.4 ± 0.1	2.95 ± 0.05	0.50 ± 0.01	4 ± 0.1
4	1.5	~0.90	4	1.45 ± 0.05	1.23 ± 0.05	1.8 ± 0.1	1.45 ± 0.05	0.85 ± 0.02	3.8 ± 0.1
5	2.5	~1.35	4	2.45 ± 0.05	1.82 ± 0.06	2.1 ± 0.1	2.45 ± 0.05	1.39 ± 0.03	3.6 ± 0.1

3D Hough accumulator are dt = 0.1 ns, dx = 5 cm, d ε = 0.1. Fig. 6 shows the results of both methods; with the curves that match the diffraction curves and the estimations of their associated parameters.

It can be observed that in the hypothesis of mathematic hyperbolas (classic Hough transform- Fig. 6 left), all 5 diffraction curves are detected at the correct apex time delays and horizontal distance. However, because the Hough transform fits to the diffraction curves with a perfect hyperbola, the estimation of the dielectric permittivity, and thus of the depth of the reflector, is erroneous. Values of 1.3 ± 0.1, 1.8 ± 0.1, 2.0 ± 0.1, 2.1 ± 0.1 and 2.3 ± 0.1 instead of 4 are found for the dielectric permittivity, leading to depth estimations of 0.85 ± 0.05, 1.23 ± 0.05, 1.43 ± 0.05, 1.82 ± 0.06 and 2.01 ± 0.06 m (to be compared to the true depths in Table 1). Thus, the depth of the reflectors is systematically overestimated, which would be an issue in the context of the ExoMars mission, as a potential hazard for the drill would be considered deeper than it is in reality and as the sample acquisition might miss the targeted geological unit.

Using the corrected Hough transform, all diffraction curves are also well detected and fitted, and the estimated dielectric permittivity values are much closer to the expected value of 4, with values of 4.0 ± 0.1, 3.8 ± 0.1, 4.2 ± 0.1, 3.6 ± 0.1 and 3.8 ± 0.1. As a consequence, the estimated depth of the reflectors is also much closer to the expected values, with depths of 0.50 ± 0.01, 0.85 ± 0.02, 0.99 ± 0.02, 1.39 ± 0.03 and 1.56 ± 0.03 m. The associated errors are in the order of a few centimetres only; 6 cm for the deepest reflector at 1.5 m below the surface.

In the above example, only echoes arising from the diffraction curves, their repetitions, and the surface were considered. In order to further test the robustness of the corrected Hough transform technique, 500 randomly distributed points have been added to the edge detection results on the radargram. The resulting cloud of points is superimposed to the radargram on the left of Fig. 7.

Fig. 7 shows that, both in the case of the classical Hough transform and of its corrected version, the results are not affected by the presence of the 500 parasitic echoes; the errors on the estimation of the dielectric permittivity and thus of the depth associated with each diffraction curve remain the same (see Table 2).

As another test, we also applied the corrected Hough transform technique to synthetic radargrams generated for heterogeneous subsurfaces with embedded reflectors (at the same locations as in Fig. 4). Indeed, variations in the dielectric permittivity of the Martian subsurface of a size comparable to WISDOM wavelengths can be expected. Such heterogeneities in the subsurface will impact the shape of the diffraction curves as modelled in section II.2.

Fig. 8 presents a synthetic radargram obtained for a heterogeneous subsurface. The heterogeneities have a fractal structure, they are generated using the Diamond-Square algorithm (Miller, 1986). The resulting distribution of dielectric permittivity values is gaussian with an of average 4, with variations between 3.5 and 4.5. We selected 16.6 cm as the characteristic size of heterogeneities, as it is of the same order as that of the reflector diameter, and around twice the central wavelength of WISDOM for a dielectric permittivity of 4. As expected, the deeper the

Table 2
Dielectric permittivity, horizontal positions and equivalent depths in the subsurface of the buried reflectors of the mode, along with Hough transform estimations for the radargram in Fig. 7.

	True values			Classic Hough transform estimation			Corrected Hough transform estimation		
N°	X (m)	Z (m)	ε	X (m)	Z (m)	ε	X (m)	Z (m)	ε
1	1	1	4	0.95 ± 0.05	1.47 ± 0.05	1.9 ± 0.1	0.95 ± 0.05	1.04 ± 0.02	3.8 ± 0.1
2	2	1.5	4	1.95 ± 0.05	2.00 ± 0.06	2.3 ± 0.1	1.95 ± 0.05	1.56 ± 0.03	3.8 ± 0.1
3	3	0.5	4	2.95 ± 0.05	0.88 ± 0.05	1.3 ± 0.1	2.95 ± 0.05	0.50 ± 0.01	4 ± 0.1
4	1.5	~0.90	4	1.45 ± 0.05	1.23 ± 0.05	1.8 ± 0.1	1.45 ± 0.05	0.85 ± 0.02	3.8 ± 0.1
5	2.5	~1.35	4	2.45 ± 0.05	1.78 ± 0.05	2.2 ± 0.1	2.45 ± 0.05	1.37 ± 0.03	3.7 ± 0.1

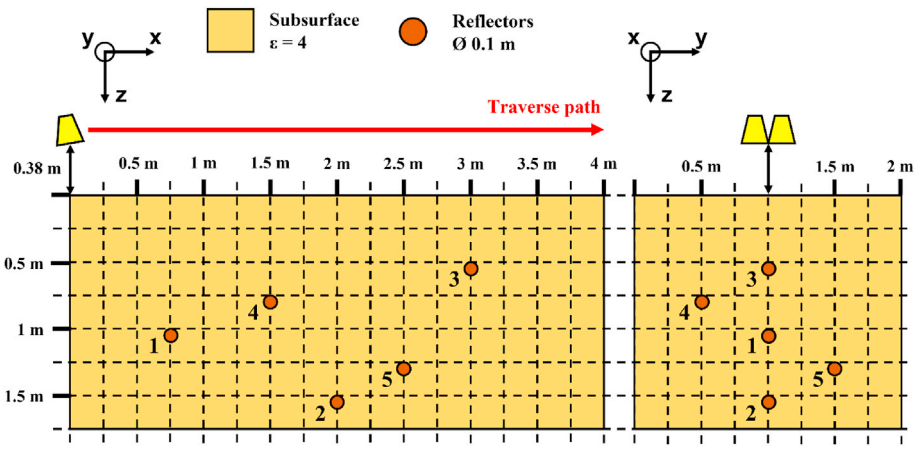

Fig. 4. Geometry of the subsurface model used for our FDTD simulations.

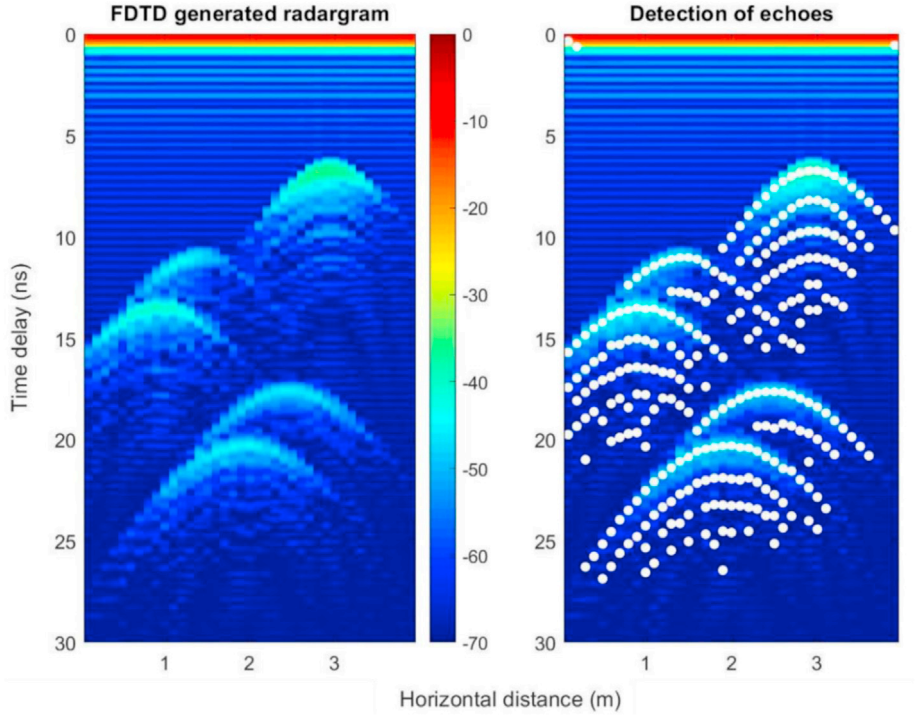

Fig. 5. Synthetic WISDOM radargram obtained by FDTD simulations (on the left), and result of the edge detection applied to this radargram (on the right).

reflector, the more the shape of its diffraction curve is affected by constructive and destructive interferences from heterogeneities.

Using the same precisions on t, X and ε as in Figs. 6 and 7 for the 3D accumulator, the deepest diffraction curve is not detected by the technique. Its detection indeed requires degrading the precisions to dt = 0.2 ns, dx = 10 cm and d ε = 0.25. These step values should therefore ideally be chosen according an *a priori* knowledge of the subsurface heterogeneity. With these values, we observe that the secondary echo of the diffraction curve corresponding the sphere number 1 (Fig. 8 right, in dashed line) is also detected by the Hough transform. But more importantly, it can be noted that all estimated dielectric permittivity values remain within the range of the expected values that is between 3.5 and 4.5. The estimated depth of reflectors are 0.50 ± 0.04 m, 0.80 ± 0.04 m, 1.09 ± 0.06 m, 1.34 ± 0.06 m and 1.48 ± 0.06 m. Such results are within about 10 cm of the input values (see Table 3) as expected due to the variations of the subsurface dielectric permittivity.

We validated in this section the Hough transform introduced in section III, on FDTD simulated WISDOM radargrams, generated using a representative 3D model of WISDOM antennas, as well as a representative model of the WISDOM transmitted signal. Despite the simplicity of the diffraction curve model the Hough transform is based on (see Fig. 2), satisfactory estimations of the 5 buried reflectors position and of the homogeneous subsurface permittivity are obtained. The presence of randomly distributed points in the edge detection have a very limited impact on these results, and the presence of a heterogeneous subsurface with permittivity values between 3.5 and 4.5 still yields reflectors depth estimations within 10 cm of the true value. Nevertheless, the subsurface model used to generate our FDTD simulated radargrams is in several aspects limited (shape and composition of the reflectors, surface roughness). The next logical step in the validation of the Hough transform is therefore its application to experimental WISDOM radargrams.

5. Validation on experimental WISDOM radargrams

The corrected Hough transform technique is validated in this section on experimental WISDOM radargrams, acquired above a subsurface of

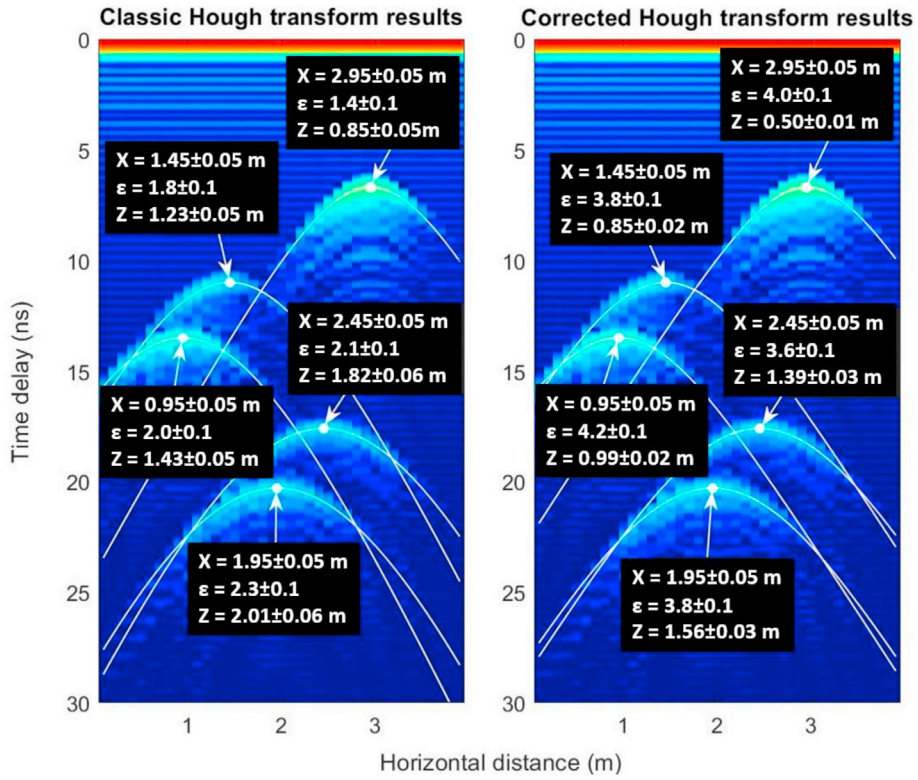

Fig. 6. Diffraction curves detected in WISDOM synthetic radargram when not accounting for refraction at the surface (on the left), and when accounting for refraction at the surface (on the right). Precisions: dt = 0.1 ns, dx = 5 cm, d ε = 0.1.

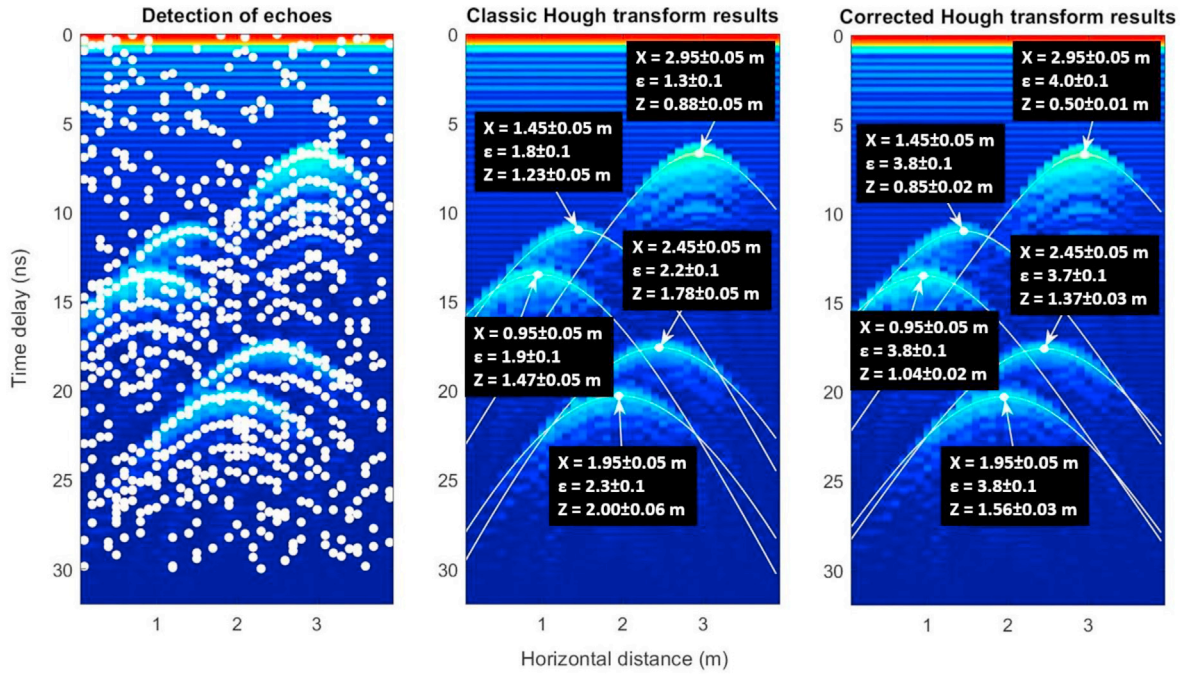

Fig. 7. Result of the edge detection applied to the synthetic radargram with the addition of 500 randomly located parasitic detections (on the left), diffraction curves detected in the synthetic radargram when not accounting for refraction at the surface (in the middle), and when accounting for refraction at the surface (on the right). Precisions: dt = 0.1 ns, dx = 5 cm, d ε = 0.1.

well constrained dielectric properties. Actually, the technique was first applied on diffraction curves resulting from calibration reflectors in free-space, for which the dielectric permittivity is expected to be 1 (Oudart, 2021). However, since no refraction effect is involved for a reflector in free-space, the corrected Hough transform technique could not be fully validated with such experimental data.

We selected data acquired during the "Dachstein Mars Simulation" field campaign organized in April 2012 by the Austrian Space Forum (Groemer et al., 2012). The campaign took place in the Dachstein Giant Ice Caves site, in Austria. GPR traverses were performed over different

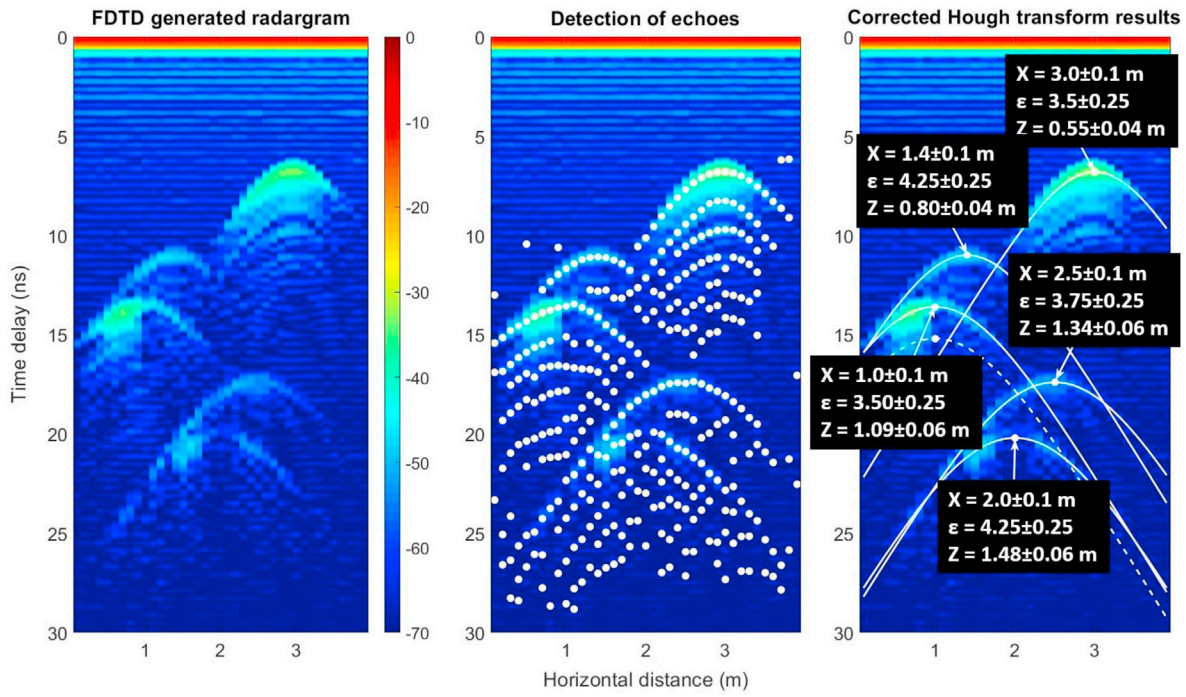

Fig. 8. Synthetic radargram generated for a heterogeneous subsurface of mean dielectric permittivity 4 (on the left), result of the edge detection applied to the this radargram (in the middle), result of the corrected Hough transform on this radargram (on the right). Precisions: dt = 0.2 ns, dx = 10 cm, d ε = 0.25.

Table 3
Dielectric permittivity, horizontal positions and equivalent depths in the subsurface of the buried reflectors of the mode, along with Hough transform estimations for the radargram in Fig. 8.

	True values			Classic Hough transform estimation			Corrected Hough transform estimation		
N°	X (m)	Z (m)	ε	X (m)	Z (m)	ε	X (m)	Z (m)	ε
1	1	1	4 ± 0.5	1.0 ± 0.1	1.48 ± 0.12	2.00 ± 0.25	1.0 ± 0.1	1.09 ± 0.06	3.50 ± 0.25
2	2	1.5	4 ± 0.5	2.0 ± 0.1	1.96 ± 0.12	2.50 ± 0.25	2.0 ± 0.1	1.48 ± 0.06	4.25 ± 0.25
3	3	0.5	4 ± 0.5	3.0 ± 0.1	0.86 ± 0.11	1.50 ± 0.25	3.0 ± 0.1	0.55 ± 0.04	3.50 ± 0.25
4	1.5	~0.90	4 ± 0.5	1.5 ± 0.1	1.20 ± 0.11	2.00 ± 0.25	1.4 ± 0.1	0.80 ± 0.04	4.25 ± 0.25
5	2.5	~1.35	4 ± 0.5	2.5 ± 0.1	1.78 ± 0.13	2.25 ± 0.25	2.5 ± 0.1	1.34 ± 0.06	3.75 ± 0.25

water ice ponds, with a prototype of the WISDOM instrument mounted on a kart. Different structures of interest were identified in the resulting radargrams, such as the layering of the ice sheet, the bedrock at the bottom of the ponds, and diffraction curves likely originating from rocks trapped in the ice (Dorizon et al., 2016).

We recall that the dielectric properties of pure water ice are well constrained at the WISDOM frequencies, with a dielectric permittivity between 3.1 and 3.2 (Fletcher, 1970). In an initial analysis of the Dachstein Mars Simulation data acquired by WISDOM, diffraction curves were manually fitted with a ray-tracing model considering refraction at the surface (Dorizon et al., 2016). Most inferred dielectric permittivity values are between 3 and 4, pointing to reflectors in water ice. A few estimations are also around 1, indicative of reflectors in the air above the surface, or between 6 and 7, indicating reflectors in the bedrock. During this previous study, the dielectric permittivity of the near-surface was also estimated from the surface echo, with a measured value of 3.2 ± 0.25. We applied the corrected version of the Hough transform to portions of radargrams with diffraction curves previously identified as arising from reflectors trapped in the ice.

Fig. 9 displays the Dachstein radargram we selected; it presents a clear diffraction curve extending upon 24 radar traces, and not interfering much with other echoes. As shown on the right of Fig. 9, the diffraction curve is correctly detected and fitted for an estimated dielectric permittivity of 3.2 ± 0.1, which is exactly the expected value for nearly pure water ice, and matches the estimation made by Dorizon et al. (2016). In contrast, when applied, the classic Hough transform (which does not account for refraction at the surface) provides a lower dielectric permittivity estimation of 2.5 ± 0.1. The depth of the reflector estimated by the corrected Hough transform technique is thus 2.27 ± 0.04 m (against 2.57 ± 0.06 m for the classic Hough transform, 20 cm deeper).

Though very satisfying, this result was somewhat expected as the diffraction curve analyzed in Fig. 9 is very clear and extends on more than 2 m in horizontal distance. We therefore also apply the corrected Hough transform technique to radargrams exhibiting several diffraction curves, extending on a small number of radar traces, and interfering with other echoes. Fig. 10 shows such a radargram, where several diffraction curves are present (at least 3), but extending on short horizontal distances (around 1 m or less, corresponding to 10 or less radar traces 10 cm apart), interfering with other echoes, and with only half of the diffraction curve visible in some cases.

First, it can be noted that the two diffraction curves clearly visible in the radargram around (1.5 m, 21 ns) and (2.8 m, 17 ns) are well detected by the technique (Fig. 10, right). A less clear diffraction curve is also identified around (1.3 m, 20 ns); its actual presence is plausible when looking at the edge detection (Fig. 10, middle). For all three diffraction curves, the estimated dielectric permittivity is consistent with water ice and previous estimates from Dorizon et al. (2016), with values around 3 and 4. A dielectric permittivity of 3.2 being valid for pure water-ice at WISDOM's frequencies, slightly higher values could be explained by lithic

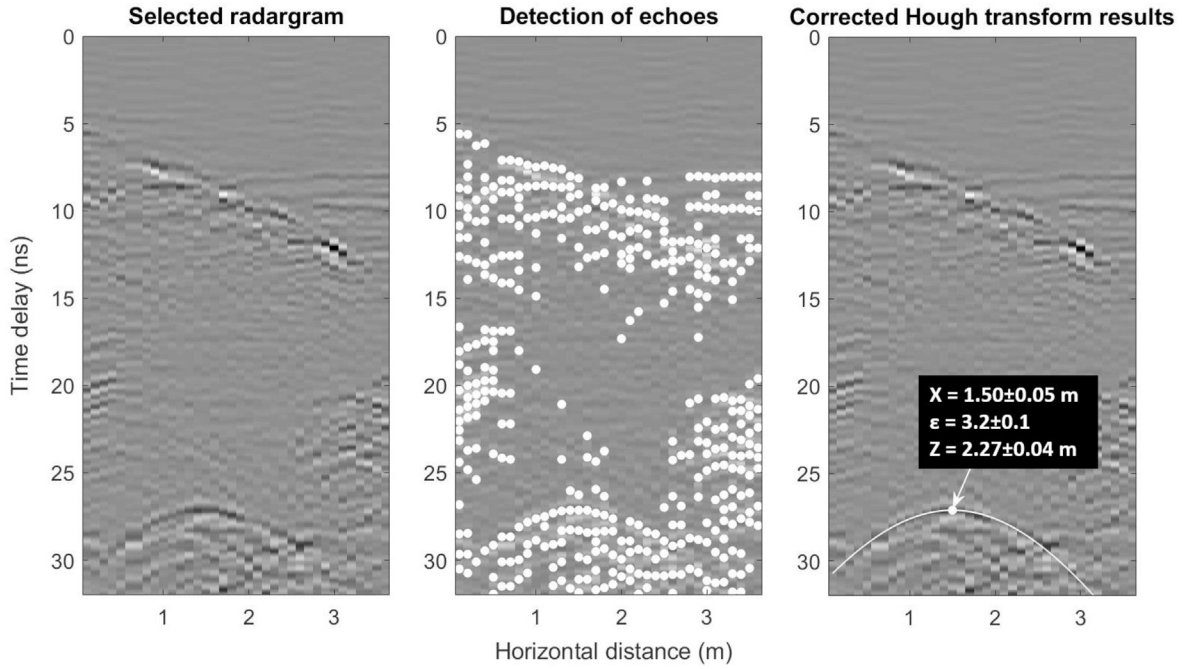

Fig. 9. First selected radargram acquired during the Dachstein Martian Simulation campaign (on the left), result of the edge detection (in the middle), result of the corrected Hough transform technique (on the right). Precisions: dt = 0.1 ns, dx = 5 cm, d ε = 0.1.

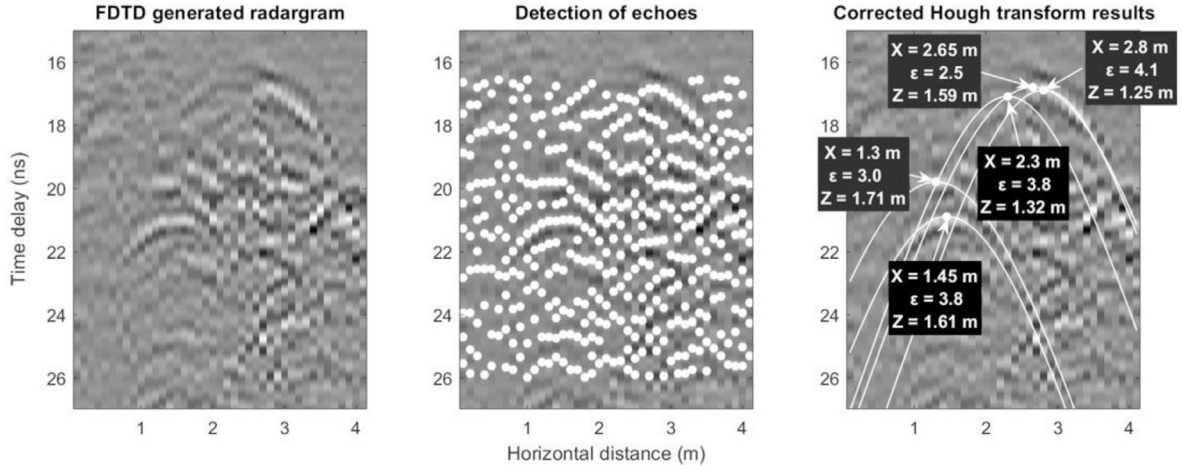

Fig. 10. Second selected radargram acquired during the Dachstein Martian Simulation campaign (on the left), result of the edge detection (in the middle), result of our Hough transform technique (on the right). Precisions: dt = 0.1 ns, dx = 5 cm, d ε = 0.1.

inclusions in the ice. In addition, the three diffraction curves are clearly interfering with other echoes. This could affect their shape and lead to dielectric permittivity estimation errors. Another factor potentially affecting the estimation is the presence of only half a diffraction curve in some cases.

For the diffraction curve at (2.8 m, 17 ns) which has only one visible branch, the corrected Hough transform returns a second detection at nearly the same position, trying to fit it with points on the left which are clearly not part of the diffraction curve. This incorrect fit results in an estimated dielectric permittivity of 2.5 $\pm$ 0.1, lower than that expected for both water ice and the bed rock, and in disagreement with results from previous studies. Another diffraction curve is detected around (2.3 m, 17 ns); as no diffraction curve is clearly visible at this location, it could be a false-positive. However, it is possible that the technique allows the detection of diffraction curves that are not visible by a simple visual inspection because located among many other echoes. As a matter of fact, this latter detection leads to an estimated dielectric permittivity close to that of water ice (3.8).

6. Discussion and perspectives

In this work, we propose an automated technique based on the Hough transform to detect diffraction curves in air-coupled GPR radargrams. The detected diffraction curves are characterized in order to estimate the dielectric permittivity of the subsurface around buried scatterers, in the hypotheses of non-magnetic and low loss-tangent materials. Air-coupled GPR being integrated to all 4 Lunar and Martian robotic rovers launched since 2013, and to the future ExoMars rover mission, such a tool is useful for the interpretation of the radargrams acquired on the Moon and on Mars in the last and next years to come.

In the context of planetary GPR missions, an accurate estimation of the subsurface dielectric properties is of prime importance as it is required to convert echoes time-delays into distances. The dielectric properties of a material also provide insights into its composition, and

thus on the geological context of a given site of exploration. In the specific frame of the ExoMars rover mission, the WISDOM instrument is to guide the drilling operations, which will collect samples down to 2 m of depth (Vago et al., 2017). WISDOM will help identify a relevant and safe drilling location since, in addition to the estimation of the dielectric permittivity, the detection of diffraction curves will allow the ExoMars rover to avoid potential subsurface hazards, such as buried rocks.

6.1. Discussion

We validated the technique we propose on both synthetic and experimental WISDOM radargrams, demonstrating the imperative need of considering refraction at the surface.

FDTD simulations were used to generate synthetic WISDOM radargrams for which the geometry of the antennas and the WISDOM transmitted signal are accurately modelled. We were thus able to confirm the validity of the technique on such realistic WISDOM GPR signal simulations. In the case of a homogeneous loss-less subsurface with a smooth surface, the estimated error on the depth of the reflectors is, at worse, of 6 cm at 1.5 m, which is quite satisfactory. However, this subsurface model is relatively simple, and not representative of the expected Martian subsurface. Nevertheless, the method was also applied with success on a heterogeneous subsurface which is a first step towards validations on more complex subsurface models.

Finally, the technique was validated on an experimental dataset acquired on a subsurface consisting of water ice, whose the dielectric permittivity value is known. Comparison against results obtained by manual fits shows that the results obtained automatically by the proposed method are very satisfying, with inferred permittivity values consistent with laboratory measurements and previous estimates. However, in more complex cases where many diffraction curves are half-visible and/or interfering with other echoes, false positives can appear. A human validation of the detections is thus required after application of the technique. Such final validation could also be done objectively and automatically by calculating the correlation between each detected diffraction curve and the radargram. Unfortunately, this natural environment not allowing any digging operations, ground truth is not available to allow a final validation of the estimated targets location. In addition, it is important to acknowledge that icy environments such as this one are very favorable for GPR soundings, leading to diffraction curves clearer than would be expected in a lithic subsurface. In contrast, GPR soundings in non-icy natural environments on Earth are often affected by moisture, which may reduce the size of diffraction curves compared to what could be expected on a similar environment on Mars. Nevertheless, further applications of the here proposed corrected version of the Hough technique should be performed on radargrams acquired in other types of environments.

The technique we propose being based on a simple geometrical model for point-like reflectors in an homogeneous subsurface, some limitations can be foreseen:

- The technique is only valid for the first subsurface layer sounded by the GPR, and the presence of a clear interface between the surface and the diffraction curve should alert us that the technique is not applicable in such case.
- It has been only tested for non-magnetic and low-losses materials. The results can be somewhat affected by heterogeneities in the subsurface (depending on their size with respect to the GPR wavelengths), or by a gradient of dielectric permittivity. The effect of heterogeneities on the technique performance deserves further investigation.
- The accuracy of the detection/characterization of diffraction curves is also expected to be impaired when the reflector is very shallowly buried. In such case, the corresponding diffraction curve will contain very few points, and be very close in shape to a hyperbola from a reflector in free-space. This points to the necessity of a synergy with other instruments (mainly cameras that could indicate the presence of rocks at the surface) to collect as much information on the sounded site as possible (homogeneity of the geological unit, materials expected or not to be magnetic or have high-losses).
- Surface roughness has not been considered. The extent to which the surface roughness would affect the dielectric properties retrieval from the diffraction curves is driven by the roughness metrics compared to the GPR wavelengths of operation. WISDOM operates at frequencies between 0.5 and 3 GHz, thus wavelengths between 10 and 60 cm in the air. According to the Rayleigh criterion, a surface can be regarded as smooth for WISDOM if the standard deviation is smaller than 1 cm. In this case, no impact on the method is to be expected. If the variations of height are larger than the wavelength and take place over a horizontal scale with a order of magnitude of several tens of centimeters, they can be considered as “topography”. The digital elevation model built by the rover's cameras together with the recorded rover attitude will allow to reconstruct the local geometry and correct this effect on the radargram. In an in-between configuration, surface roughness would induce a deterioration of the GPR vertical resolution, and the reduction of the diffraction curve's signal strength concomitant with an increase of the clutter. This would make diffraction curves harder to detect. In mission, the digital elevation model provided by the rover's cameras would indicate if the proposed method is compatible with the surface roughness or not.
- Eventually, a reflector too large to be considered “point-like” at the GPR wavelengths in the subsurface, or with a complicated shape, would make the diffraction curve different from the one modelled. This would cause errors in the dielectric permittivity estimations. Nevertheless, a diffraction curve too different from the model would lead to less clear peaks in the Hough accumulator, decreasing the risk of detecting it.

Some aspects of the Hough transform technique in itself can be discussed. The 3 mains are:

- The edge detection we apply to the radargrams is a simple peak detection, with a threshold on the peak intensity. A large amount of detected points is useful to the Hough transform, but at the expense of computation time. Time allocated to WISDOM processing being limited by the ExoMars mission constraints, the threshold is currently selected to account for an acceptable number of points, leading to an acceptable computing/processing time. However, this threshold selection is arbitrary, and the technique would benefit from an objective criterion.
- When looking for peaks in the Hough 3D accumulator, we currently search for local maxima within a 3D Moore neighborhood. This way, we try to avoid multiple detections close to a hyperbolic vertex without impairing too much our ability to detect diffraction curves with vertices very close to each other. However, doing so, we probably allow multiple detections or miss overlapping diffraction curves (see Capineri et al., 1998). For the tests shown in this article, this was not much of an issue. However, this effect is expected to become more important if we wish for more precision in the 3D Hough accumulator The technique would in this case benefit from a method to reduce such multiple detections (for an example see Gerig and Klein, 1986).
- Another point of the peaks search in the Hough 3D accumulator that could be optimized is the setting of a threshold on the peaks to be considered as diffraction curves detections. This is a delicate point in the application of any Hough transform for which probabilistic techniques have been proposed in the case of straight lines detection (Princen et al., 1990). Currently, this threshold can be set manually in our software after application of the Hough transform to the radargram. However, the technique's automation would benefit from an objective criterion.
- Finally, the precisions on the estimated horizontal position, time delays and dielectric permittivity for each diffraction curve are directly driven by the precision on each axis in the 3D accumulator.

These 3 parameters chosen by the user can impact detection: too much precision will lead to reduced peaks values in the accumulator, making them harder to detect, but not enough precision will prevent the separation of diffraction close to each other. This parameter is also selected arbitrarily, and would benefit from an objective criterion.

6.2. Perspectives

Despite the limitations discussed in the previous sub-section, the technique we proposed in this paper represents a step ahead in the interpretation of planetary GPR data, for which diffraction curves are often fitted manually, and from which the subsurface dielectric permittivity is often inferred without accounting for refraction at the surface (e.g., Lai et al., 2016). In the case of the WISDOM example, the dielectric permittivity of the first subsurface layer can also be estimated from the amplitude of the surface echo, as calibration measurements have been performed on a perfect reflector (Ciarletti et al., 2017; Dorizon et al., 2016; Hervé et al., 2020) (provided that the surface can be regarded as smooth). Unlike the estimation from the surface echo, the new technique proposed here is less affected by the surface roughness, and does not require an accurate radiometric calibration. Machine learning techniques have also been developed by the WISDOM team to detect diffraction curves in radargrams (Hervé, 2018). However, the need for a large dataset of experimental diffraction curves, so far, prevented us from applying the technique to experimental radargrams. Nevertheless, the corrected Hough transform technique could also help building a data base of diffraction curves from future Martian radargrams, to feed the machine learning algorithm we developed.

The next logical step in the validation of the corrected Hough transform technique is a thorough analysis of the effect of heterogeneities on the dielectric permittivity estimations. Further simulations and WISDOM experiments are planned over materials having heterogeneities of different sizes and different dielectric contrasts. More realistic subsurface models, with more complicated targets will also be considered. In addition, the super-resolution technique named "bandwidth extrapolation" recently implemented to the WISDOM processing chain is expected to improve the performances of the corrected Hough transform, by better separating diffraction curves from other echoes (Oudart et al., 2021). Preliminary successful tests have been conducted on diffraction curves resulting from echoes on metallic spheres in free-space. Eventually, the technique will be applied to data collected during future field campaigns, in preparation for the ExoMars rover mission on Mars (especially in the periglacial landforms of Svalbard, Norway). This will be the first application of the technique to data acquired in relevant Martian analogue environments before its application to actual ExoMars observations. Applications to other Martian GPR observation can also be foreseen, as radargrams are currently being acquired from the Martian surface by the RIMFAX and RoPeR instruments. Furthermore, preliminary results from both instruments have already been published, with subsurface dielectric permittivity estimations from diffraction curves providing insights on the geological history of the rovers' landing sites.

Author statement

Nicolas Oudart: Writing – Original Draft, Writing – Review & Editing, Conceptualization, Methodology, Software **Valérie Ciarletti:** Writing – Original Draft, Writing – Review & Editing, Methodology, Project administration, Supervision, **Alice Le Gall:** Writing – Original Draft, Writing – Review & Editing, Methodology, Supervision, **Yann Hervé:** Software, Validation, Resources, **Emile Brighi:** Software.

Declaration of competing interest

The authors declare that they have no known competing financial interests or personal relationships that could have appeared to influence the work reported in this paper.

Data availability

Data will be made available on request.

Acknowledgments

This study was funded by CNES and the Université Versailles Saint-Quentin. WISDOM is funded by CNES and DLR. The TEMSI-FD FDTD simulation software was developed by XLIM.

References

Capineri, L., Grande, P., Temple, J.A.G., 1998. Advanced image-processing technique for real-time interpretation of ground-penetrating radar images. Int. J. Imag. Syst. Technol. 9, 51–59. https://doi.org/10.1002/(SICI)1098-1098(1998)9:1<51::AID-IMA7>3.0.CO;2-Q.

Carlotto, M.J., 2002. Detecting buried mines in ground-penetrating radar using a Hough transform approach. In: Suresh, R., Roper, W.E. (Eds.), Battlespace Digitization and Network-Centric Warfare II. SPIE, pp. 251–261. https://doi.org/10.1117/12.478719.

Ciarletti, V., Clifford, S., Plettemeier, D., le Gall, A., Hervé, Y., Dorizon, S., Quantin-Nataf, C., Benedix, W.S., Schwenzer, S., Pettinelli, E., Heggy, E., Herique, A., Berthelier, J.J., Kofman, W., Vago, J.L., Hamran, S.E., 2017. The WISDOM radar: unveiling the subsurface beneath the ExoMars rover and identifying the best locations for drilling. Astrobiology 17, 565–584. https://doi.org/10.1089/ast.2016.1532.

Ding, C., Xiao, Z., Su, Y., Cui, J., 2021. Hyperbolic reflectors determined from peak echoes of ground penetrating radar. Icarus 358, 114280. https://doi.org/10.1016/j.icarus.2020.114280.

Dorizon, S., Ciarletti, V., Plettemeier, D., Benedix, W.S., 2016. Performance validation of the ExoMars 2018 WISDOM GPR in ice caves, Austria. Planet. Space Sci. 120, 1–14. https://doi.org/10.1016/j.pss.2015.10.008.

Duda, R.O., Hart, P.E., 1972. Use of the hough transformation to detect lines and curves in pictures. Commun. ACM 15, 11–15. https://doi.org/10.1145/361237.361242.

Fang, G.Y., Zhou, B., Ji, Y.C., Zhang, Q.Y., Shen, S.X., Li, Y.X., Guan, H.F., Tang, C.J., Gao, Y.Z., Lu, W., Ye, S.B., Han, H.D., Zheng, J., Wang, S.Z., 2014. Lunar penetrating radar onboard the Chang'e-3 mission. Res. Astron. Astrophys. 14, 1607–1622. https://doi.org/10.1088/1674-4527/14/12/009.

Fletcher, N.H., 1970. Liquid water and freezing. In: The Chemical Physics of Ice, pp. 73–103. https://doi.org/10.1017/cbo9780511735639.006.

Gerig, G., Klein, F., 1986. Fast Contour Identification Through Efficient Hough Transform and Simplified Interpretation Strategy (undefined).

Groemer, G., Luger, U., Juhart, K., Plettemeier, D., Hettrich, S., Sans, A., Souchier, A., Vimercati, L., Noell, A., Boehme, R., Balwant, R., Rodrigues, L., Mogosanu, H., Carbognani, F., Meszyński, S., 2012. (PDF) Dachstein Mars simulation 2012 mission report [WWW document]. URL, 7.30.20. https://www.researchgate.net/publication/235753475_Dachstein_Mars_Simulation_2012Mission_Report.

Hamran, S.E., Paige, D.A., Amundsen, H.E.F., Berger, T., Brovoll, S., Carter, L., Damsgård, L., Dypvik, H., Eide, J., Eide, S., Ghent, R., Helleren, Ø., Kohler, J., Mellon, M., Nunes, D.C., Plettemeier, D., Rowe, K., Russell, P., Øyan, M.J., 2020. Radar imager for Mars' subsurface experiment-RIMFAX. Space Sci. Rev. https://doi.org/10.1007/s11214-020-00740-4.

Hervé, Y., 2018. Le radar WISDOM à bord du Rover de la mission ExoMars : caractérisation et préparation du retour scientifique. Université de Versailles Saint-Quentin (PhD thesis).

Hervé, Y., Ciarletti, V., Le Gall, A., Corbel, C., Hassen-Khodja, R., Benedix, W.S., Plettemeier, D., Humeau, O., Vieau, A.J., Lustrement, B., Abbaki, S., Bertran, E., Lapauw, L., Tranier, V., Oudart, N., Vivat, F., Statz, C., Lu, Y., Hegler, S., Hérique, A., 2020. The WISDOM radar on board the ExoMars 2020 Rover: characterization and calibration of the flight model. Planet. Space Sci., 104939 https://doi.org/10.1016/j.pss.2020.104939.

Hervé, Yann, Ciarletti, Valerie, Le Gall, Alice, Corbel, Charlotte, Hassen-Khodja, Rafik, Wolf-Stefan, Benedix, Plettemeier, Dirk, Olivier, Humeau, André-Jean, Vieau, Lustrement, Benjamin, Abbaki, Sadok, Bertran, Emmanuel, Lapauw, Laurent, Vivien Tranier, N.O.A.H., 2020. The WISDOM radar on board the ExoMars 2020 Rover: characterization and calibration of the flight model. Planet. Space Sci. Volume 189.

Hough, P.V.C., 1964. Man - machine collaboration in the analysis of bubble chamber photography for high - energy physics. Opt. Eng. 2. https://doi.org/10.1117/12.7971269.

Jia, Y., Zou, Y., Ping, J., Xue, C., Yan, J., Ning, Y., 2018. The scientific objectives and payloads of Chang'E-4 mission. Planet. Space Sci. https://doi.org/10.1016/j.pss.2018.02.011.

Lai, J., Xu, Y., Zhang, X., Tang, Z., 2016. Structural analysis of lunar subsurface with Chang'E-3 lunar penetrating radar. Planet. Space Sci. 120, 96–102. https://doi.org/10.1016/j.pss.2015.10.014.

Lai, J., Xu, Y., Zhang, X., Xiao, L., Yan, Q., Meng, X., Zhou, B., Dong, Z., Zhao, D., 2019. Comparison of dielectric properties and structure of lunar regolith at chang'e-3 and chang'e-4 landing sites revealed by ground-penetrating radar. Geophys. Res. Lett. 46, 12783–12793. https://doi.org/10.1029/2019GL084458.

Li, W., Cui, X., Guo, L., Chen, J., Chen, X., Cao, X., 2016. Tree root automatic recognition in Ground penetrating radar profiles based on randomized Hough transform. Rem. Sens. 8, 430. https://doi.org/10.3390/rs8050430.

Miller, G.S.P., 1986. The definition and rendering of terrain maps. ACM SIGGRAPH Computer Graphics 20, 39–48. https://doi.org/10.1145/15886.15890.

Nelder, J.A., Mead, R., 1965. A simplex method for function minimization. Comput. J. 7, 308–313. https://doi.org/10.1093/comjnl/7.4.308.

Oudart, N., 2021. Assessment of Processing and Interpretation Tools in Preparation of the WISDOM/ExoMars Ground Penetrating Radar Operations on Mars. 2021. Université Paris-Saclay.

Oudart, N., Ciarletti, V., Le Gall, A., Mastrogiuseppe, M., Hervé, Y., Benedix, W.-S., Plettemeier, D., Tranier, V., Hassen-Khodja, R., Statz, C., Lu, Y., 2021. Range resolution enhancement of WISDOM/ExoMars radar soundings by the Bandwidth Extrapolation technique: validation and application to field campaign measurements. Planet. Space Sci. 197, 105173. https://doi.org/10.1016/j.pss.2021.105173.

Persico, R., Leucci, G., Matera, L., De Giorgi, L., Soldovieri, F., Cataldo, A., Cannazza, G., De Benedetto, E., 2015. Effect of the height of the observation line on the the diffraction curve in GPR prospecting. Near Surf. Geophys. 13, 243–252. https://doi.org/10.3997/1873-0604.2014042.

Princen, J., Illingworth, J., Kittler, J., 1990. Hypothesis Testing: A Framework for Analysing and Optimising Hough Transform Performance, pp. 427–434. https://doi.org/10.1109/ICCV.1990.139564.

Vago, J.L., Westall, F., Coates, A.J., Jaumann, R., Korablev, O., Ciarletti, V., Mitrofanov, I., Josset, J.L., De Sanctis, M.C., Bibring, J.P., Rull, F., Goesmann, F., Steininger, H., Goetz, W., Brinckerhoff, W., Szopa, C., Raulin, F., Edwards, H.G.M., Whyte, L.G., Fairén, A.G., Bridges, J., Hauber, E., Ori, G.G., Werner, S., Loizeau, D., Kuzmin, R.O., Williams, R.M.E., Flahaut, J., Forget, F., Rodionov, D., Svedhem, H., Sefton-Nash, E., Kminek, G., Lorenzoni, L., Joudrier, L., Mikhailov, V., Zashchirinskiy, A., Alexashkin, S., Calantropio, F., Merlo, A., Poulakis, P., Witasse, O., Bayle, O., Bayón, S., Meierhenrich, U., Carter, J., García-Ruiz, J.M., Baglioni, P., Haldemann, A., Ball, A.J., Debus, A., Lindner, R., Haessig, F., Monteiro, D., Trautner, R., Voland, C., Rebeyre, P., Goulty, D., Didot, F., Durrant, S., Zekri, E., Koschny, D., Toni, A., Visentin, G., Zwick, M., Van Winnendael, M., Azkarate, M., Carreau, C., 2017. Habitability on early Mars and the search for biosignatures with the ExoMars rover. Astrobiology. https://doi.org/10.1089/ast.2016.1533.

Windsor, C.G., Capineri, L., Falorni, P., 2005. The estimation of buried pipe diameters by generalized hough transform of radar data. In: PIERS 2005 - Progress in Electromagnetics Research Symposium, Proceedings. Electromagnetics Academy, pp. 345–349. https://doi.org/10.2529/piers041117130829.

Xu, L., Oja, E., 1993. Randomized hough transform (RHT): basic mechanisms, algorithms, and computational complexities. CVGIP Image Underst. 57, 131–154. https://doi.org/10.1006/ciun.1993.1009.

Zhou, B., Shen, S., Lu, W., Liu, Q., Tang, C., Li, S., Fang, G., 2020. The Mars rover subsurface penetrating radar onboard China's Mars 2020 mission. Earth and Planetary Physics 4, 1–10. https://doi.org/10.26464/epp2020054.